Mineralogy and Petrology (2005) 83: 1–25
DOI 10.1007/s00710-004-0062-4

Mineralogy and Petrology
Printed in Austria

Formation of corundum in metapelites around ultramafic bodies. An example from the Saualpe region, Eastern Alps

M. Riesco[1,2], **K. Stüwe**[1], and **J. Reche**[2]

[1] Institute of Earth Science, University of Graz, Austria
[2] Department of Geology, Universitat Autonoma de Barcelona, Spain

Received May 24, 2004; revised version accepted August 25, 2004
Published online October 20, 2004;
Editorial handling: *J. G. Raith*

Summary

This paper describes corundum formation in a metasomatic reaction zonation around an ultramafic body within a metapelitic sequence. The investigated body is about 100 m in diameter and is located in the Saualpe of the Austroalpine nappe complex in the Eastern Alps. The body is surrounded by a 10 m wide reaction zone (here called zone 3) containing the paragenesis garnet–staurolite–biotite–margarite–chlorite–corundum. Beyond a further metasomatic transition zone (here called zone 2), there are undisturbed metapelitic host rocks (zone 1) that have the metamorphic peak paragenesis garnet–biotite–plagioclase–staurolite–muscovite–quartz. It is shown that reaction zonation formed around 7.2 kbar and 615 °C during regional metamorphism, just above the serpentine breakdown reactions in the system $MgO–SiO_2–H_2O$. Detailed analysis of the whole rock compositions shows that the reaction zonation formed by infiltration metasomatism that caused significant mass loss in the two alteration zones. These zones are particularly depleted in SiO_2, Na_2O and possibly K_2O. An $X_{Na_2O}–X_{SiO_2}$ thermodynamic pseudosection is presented that includes the parageneses of both the unaltered metapelitic host rock and the corundum-bearing parageneses. This suggests that the metasomatic process can be explained by the transfer of SiO_2 and Na_2O alone. We interpret that the process is driven by water liberated from the previously serpentinised ultramafic body during prograde dehydration during regional Eo-Alpine metamorphism. This fluid flowed outwards from the ultramafic body depleting the surrounding pelites in silica and causing margarite formation from plagioclase and muscovite. This interpretation of the driving mechanism is consistent with our knowledge of the low water activities of the Saualpe during the Eo-Alpine orogenic cycle.

Introduction

Reaction zones at the contact between ultramafic bodies and their country rocks are common examples of metasomatism during regional metamorphism (*Sanford*, 1982; *Carswell* et al., 1974; *Pfeifer*, 1987; *Bebout* and *Barton*, 2002). Most of these studies describe silica depletion of aluminous schists or metabasites caused by their proximity to an ultramafic body. However, interestingly, none of these authors have described the formation of corundum as a result of silica-depletion during this process. Except for the studies of *Simandl* and *Paradis* (e.g. 1999) and *Surour* and *Arafa* (1997), we are not aware of any descriptions of corundum-bearing rocks that formed during metasomatism between ultramafic rocks and their host rocks. Most modern petrological descriptions of corundum formation are in association with silica-rich rocks: for example those that describe corundum occurrences in high-T terrains where the assemblage corundum + quartz becomes stable (*Shaw* and *Arima*, 1998), silica depletion during melting (*Cartwright* and *Barnicoat*, 1986; *Riesco* et al., 2004); descriptions of corundum near contacts between mafics and marbles (*Lopez* and *Soto*, 2002); or corundum associated with staurolite or margarite (*Emani* and *Zang*, 1988; *Ranson* and *William*, 2000).

In this paper we provide a detailed description of corundum formation at the contact between an ultramafic body and its surrounding metapelites in the Eastern Alps in Europe. The primary focus of this study is to document the formation conditions and bulk compositional variation across the zonation that led to the formation of corundum-bearing parageneses. We will then use this information to interpret some aspects of the formation process and migration paths during metasomatism.

Regional geology

The ultramafic body we describe here is located in the Saualpe region of the Eastern Alps, which also hosts the eclogite type locality (*Hauy*, 1822; *Miller*, 1990; *Habler* and *Thöni*, 2001; *Thöni* and *Miller*, 1996; *Tenczer* and *Stüwe*, 2003). More specifically, it is located within the Plankogel series, which is a cover series structurally above the eclogite facies rocks (Fig. 1a). The Plankogel series and the underlying units experienced amphibolite and eclogite facies metamorphism during the Eo-Alpine orogenic cycle in the Cretaceous, respectively (*Gregurek* et al., 1997; *Stüwe*, 1998; *Frey* et al., 1999). Rocks in the Plankogel series are characterized by coarse grained staurolite–garnet mica-schists that include tectonically emplaced lenses of marbles, amphibolites, manganese–quartzites and ultramafic rocks that are up to kilometers in size (*Frisch* et al., 1989; *Weissenbach*, 1975; *Schmerold*, 1988). Most of the ultramafic bodies are now present as serpentinites and have normative compositions of harzburgites, lherzolites, olivine orthopyroxenites and olivine websterite (*Schmerold*, 1988; *Frisch* et al., 1989). The ultramafic body investigated here is some 100 meters in diameter and is well known by mineral collectors as the ''Lölling occurrence'' for its coarse grained occurrences of garnet and corundum (*Meixner*, 1967). These and other minerals formed at the contact between the ultramafic body and the surrounding metapelites. Minerals formed in the contact zones obliterate the regional Eo-Alpine fabric indicating that the zones formed during the Eo-Alpine metamorphic cycle. Although there is

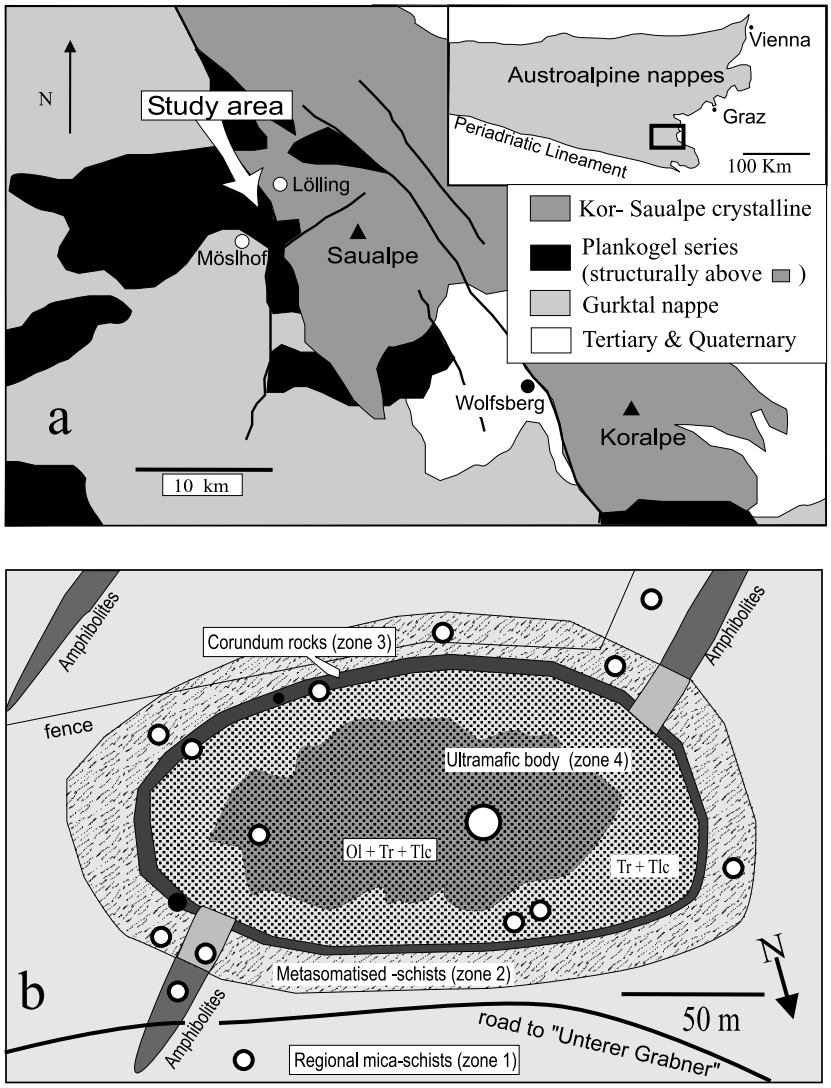

Fig. 1. **a** Simplified geological map of the location and regional geology of the study area (modified after *Schuster* and *Frank*, 2000). The marked study area location is at E 14°34′07″ N 46°54′28″, just south of the Lölling valley, which is a contributory to the Görtschitz valley. The nearest homestead to the study area is called ‘‘Unterer Grabner’’. **b** Interpreted schematic map of the contact aureole under investigation inferred from the few available outcrops (white dots)

little outcrop (and individual outcrops are typically only about 1–2 m^2 in size), a characteristic zoning of rock types can be recognized over a distance of some tens of meters between the ultramafic body and the country rock (Fig. 1b).

Petrography and mineral chemistry

Based on mineralogy, four different zones may be discerned around the Lölling ultramafic body (Fig. 1b). Although outcrop conditions are too poor to verify a

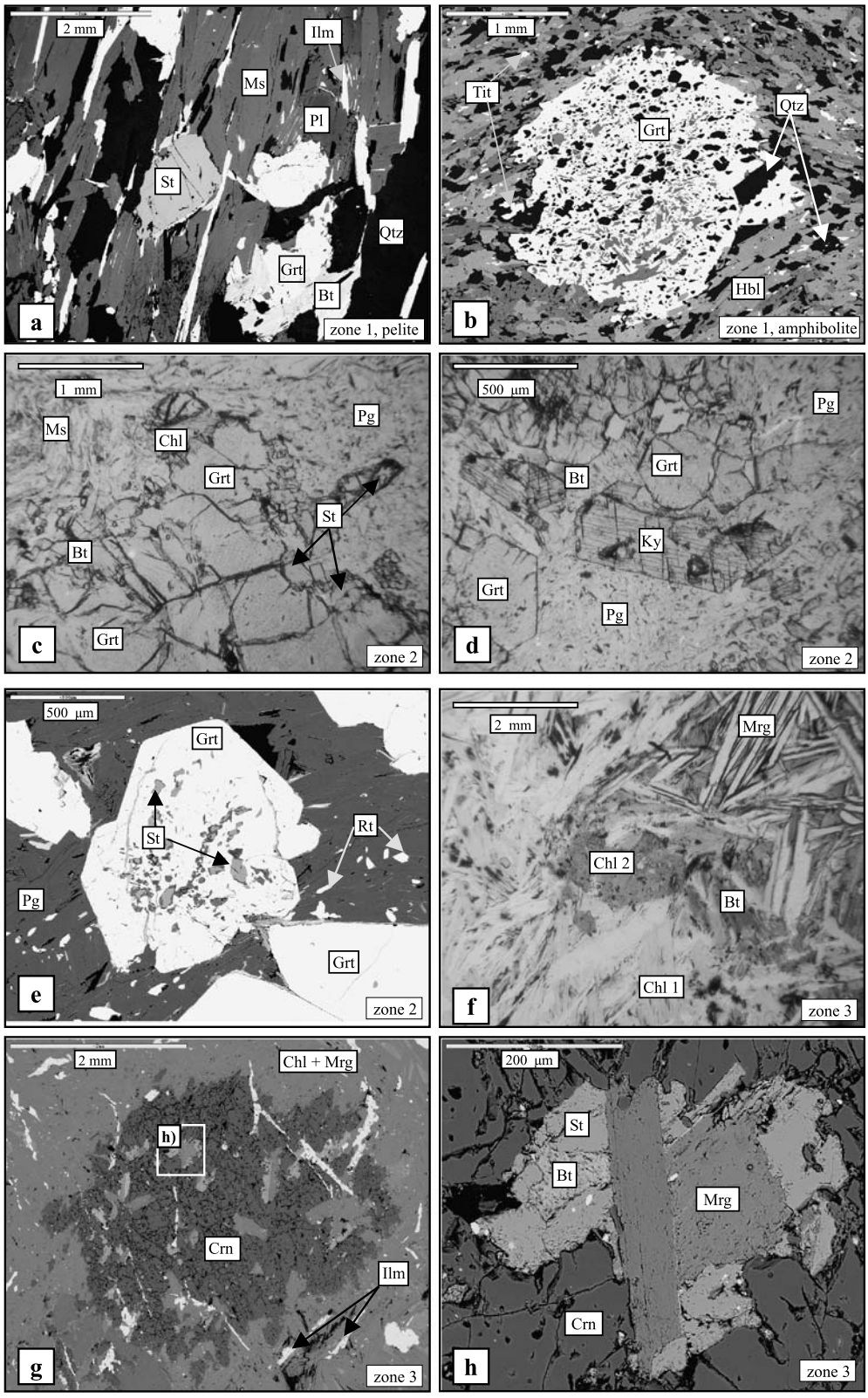
2 mm
Ilm
Ms
Pl
St
Qtz
Grt
Bt
a
zone 1, pelite
1 mm
Tit
Qtz
Grt
Hbl
b
zone 1, amphibolite
1 mm
Ms
Chl
Pg
Grt
St
Bt
Grt
c
zone 2
500 µm
Pg
Bt
Grt
Ky
Grt
Pg
d
zone 2
500 µm
Grt
St
Rt
Pg
Grt
e
zone 2
2 mm
Mrg
Chl 2
Bt
Chl 1
f
zone 3
2 mm
Chl + Mrg
h)
Crn
Ilm
g
zone 3
200 µm
St
Bt
Mrg
Crn
h
zone 3

concentric pattern of these zones, their zonation follows a characteristic distribution with distance from the ultramafic body. The outermost zone (zone 1) is the unaltered country rock of the Plankogel series. In the vicinity of the Lölling occurrence the rocks in this zone are mostly mica-schists, but also contain some amphibolites and marbles. The next zone (zone 2) is referred to as metasomatized schists. It contains slightly altered country rocks that may or may not be quartz absent. This zone also contains lenses of metasomatized amphibolites. The third zone (zone 3) contains corundum-bearing rocks that are the focus of this study. Finally, the fourth and innermost zone (zone 4) is the ultramafic body itself. It contains rocks derived from serpentinites of the Plankogel series. Some samples (near the country rock) are only composed of tremolite and talc, others (nearer the center of the ultramafic body) also contain some olivine, giving a vague appearance of a change in alteration with distance from the center. In the following sections we describe the petrography and chemistry of each zone (Fig. 2, Tables 1, 2). Descriptions of the amphibolites and mica-schists in the undisturbed region (zone 1) may also be found by *Habler* and *Thöni* (2001) and references therein.

Zone 1: Mica-schists and amphibolites

The Plankogel mica-schists of zone 1 show a schistosity generated during regional metamorphism (Fig. 2a). The three most important assemblages observed are (Table 1): Qtz + St + Grt + Bt + Pl + Ms + Ilm (represented by samples *Sau7* and *Sau8*); Qtz + Ky + St + Grt + Bt + Pl + Ms + Ilm (*Sau11*) and Qtz + Grt + Bt + Pl + Ms + Ilm + Rt (*Sau12*). Subhedral garnet porphyroblasts are common in all the assemblages and vary in size between 0.5 mm and 4 mm. $X_{Fe} = Fe/(Fe + Mg)$ ratios in garnet from different samples are between $X_{Fe} = 0.79$ to 0.82. Garnet grains have homogeneous composition with a narrow rim where X_{Fe} increases up to 0.84. Staurolite occurs as subhedral grains of millimetre size in both the assemblages of samples *Sau7*, *Sau8* and that of *Sau11*. Staurolite crystals are chemically homogeneous with $X_{Fe} = 0.80$ to 0.84. Biotite, which is present in all the assemblages, appears always oriented parallel to the schistosity of the rock (Fig. 2a). Chemical analysis show a high variability with X_{Fe} between 0.43 and 0.50. Titanium content of biotites is around 1 wt%. Plagioclase is generally slightly zoned. Na/(Na + Ca) ratios range from 0.20 to 0.35. The only white mica present in these assemblages is muscovite with Na/(Na + K) = 0.20 to 0.17. Ilmenite is the

Fig. 2. Representative photomicrographs of characteristic assemblages of the metasomatic aureole. Mineral abbreviations after *Kretz* (1983). **a** and **b** Examples of the country Plankogel series rocks (zone 1). **a** Example of mica-schist with a dominant foliation defined by micas; **b** shows an amphibolite with coarse garnet poikiloblast. **c**, **d** and **e** Metasomatized schists (zone 2). Note the appearance of randomly oriented paragonite, kyanite and euhedral garnet. **e** Garnet with trails of staurolite inclusions. **f**, **g** and **h** Examples from the corundum-bearing rocks of zone 3. **f** Staurolite replaced by chlorite (centre of micrograph). **g** Corundum porphyroblast with inclusions. **h** shows is detail of **g** showing an inclusion cluster of margarite, staurolite and biotite

Table 1. *Mineral assemblages of the rock types in the study area. Mineral abbreviations after* Kretz *(1983).* X *Part of the peak assemblage;* o *mineral present in small proportion or relic,* R *retrograde mineral. The two parageneses used for Fig. 3b and c are printed in bold. Sample numbers shown in italics are samples for which XRF whole rock analyses are given in Table 3.* PT *indicates assemblages used for the average* PT *calculations on Fig. 5a*

Zone 1: country rock																
Mica-schists																
#		Qtz	Crn	Ky	St	Grt	Bt	Chl	Plag	Zo	Ms	Marg	Pg	Tour	Ilm	Rt
Sau7		X			X	X	X		X		X				X	
Sau8	PT	X			X	X	X		X		X			X	X	
Sau11	PT	**X**		**X**	**X**	**X**	**X**	**R**	**X**		**X**				**X**	**o**
Sau12		X				X	X		X		X				X	o
amphibolites																
#		Qtz	Plag	Hbl	Grt	Omp	Chl	Rt	Sph	Zo						
Sau9	PT	X		X	X			o	X	X						
Sau14a		X		X	X			X								
Sau14b		X	X	X	X	o		X								
Zone 2: metasomatic zone																
metasomatic schists																
#		Qtz	Crn	Ky	St	Grt	Bt	Chl	Plag	Zo	Ms	Marg	Pg	Tour	Ilm	Rt
Sau16		X			X	X	X		X		X				X	
Sau5	PT	X			X	X	X	R	X		X		X	o	X	X
Sau4		o			X	X	o	R	X		X			X	X	
Sau13				X	X	X	o				X				X	
Sau15b				X	X	X	X				X					
Sau22				X	X	X	X				X		X		X	X
Sau3	PT			X	X	X	X						X		X	
metasomatic amphibolite																
#		Qtz	Plag	Hbl	Grt	Omp	Chl	Rt	Sph	Zo						
Sau21				X	X		X	X		X						
Zone 3: corundum rocks																
Corundum bearing rocks																
#		Qtz	Crn	Ky	St	Grt	Bt	Chl	Plag	Zo	Ms	Marg	Pg	Tour	Ilm	Rt
Sau1			X			X		X		X		X			X	
Sau2			**X**		**o**	**X**	**o**	**X**, **R**				**X**			**X**	
Sau2b			**X**		**o**	**X**	**X**	**X**, **R**				**X**			**X**	
Sau2c	PT		**X**		**o**	**X**	**X**	**X**, **R**				**X**			**X**	
Sau15a			X		o	X	X	X, R				X			X	
Sau19			X					X				X			X	
Zone 4: intrusion																
Ultramafic rocks																
#		Ol	Spl	Tlc	Atg	Tr	Chl									
Sau10		X	o		R	X										
Sau18		X		X	R	X	o									
Sau20		X			R	X	X									
Sau6			X		X	o										
Sau17			X		X											

common titanium oxide although rutile has also been observed in one sample. Kyanite occurs as anhedral porphyroblasts in the assemblage of *Sau11*.

The amphibolite lenses in zone 1 are aligned in the regional fabric but have only a weakly developed schistosity. Several different assemblages were sampled in the amphibolites (Table 1). All of them contain poikiloblastic garnets (Fig. 2b). Zoisite and plagioclase occur in the matrix and as inclusions in garnet in some rocks and some assemblages contain clinopyroxene. The common titanium phases are rutile and titanite. Where the amphibolites are metasomatized in zone 2 they show a randomly oriented texture and are often quartz-free. Some assemblages include alumina-bearing phases such as chlorite. Garnet is present as subhedral grains. Coarse grained amphiboles in the metasomatized amphibolites of zone 2 have a higher alumina/silica ratio than in the amphibolites of zone 1 (samples *Sau9* and *Sau21* in Table 2a). Garnet in the metasomatized amphibolites in zone 2 has higher magnesium content ($X_{Py} = Mg/(Mg + Ca + Fe + Mn) = 0.21$) than those in zone 1 ($X_{Py} = 0.09$). In the amphibolites in zone 2 zoisite is only present as inclusions in garnet, suggesting that it was extracted from the matrix during metasomatism.

Zone 2: Metasomatized schists

Zone 2 is a transition zone between the country rocks and the corundum-bearing rocks. It contains rocks of a range of bulk compositions. A common feature of all rocks in this zone is a relic layered anisotropy inherited from the parent mica-schists. However, foliation is less penetrative than that of rocks in zone 1 and the fabric is locally randomly oriented (Fig. 2c, d). The following assemblages are observed (in an approximate order from country rock towards the ultramafic body) (Table 1): Qtz + St + Grt + Bt + Pl + Ms + Ilm ± Pg (*Sau5*, *Sau16*); Ky + St + Grt + Bt + Ms + Ilm ± Pg (*Sau13*, *Sau15b*, *Sau23*) and: Ky + St + Grt + Bt + Pg + Ilm (*Sau3*). Quartz is scarce and concentrated in bands in the first of these three assemblages. Paragonite appears locally as random oriented aggregates. The rest of the phases are similar both chemically and texturally to those in the country mica-schists of zone 1. Biotite is scarce and new staurolite ($X_{Fe} = 0.84$) is formed from garnet (Fig. 2c). In the most strongly altered samples, quartz, muscovite and plagioclase are absent whereas randomly oriented fibrous paragonite crystals are the main constituents (Fig. 2d). Paragonite is high in calcium with $Ca/(Ca + Na) = 0.13$ and little potassium with $K/(K + Ca + Na) = 0.06$. Euhedral garnet porphyroblasts (Fig. 2e) contain inclusion trails of staurolite. Interestingly, staurolites included in garnets have low iron content ($X_{Fe} = 0.63$) compared to staurolite in zone 1. Other phases included in the garnet porphyroblats are rutile, ilmenite and biotite. Biotite is scarce in the matrix in places where 20–50 μm sized rutile crystals are common (Fig. 2e).

Zone 3: Corundum-bearing rocks

Zone 3 is characterized by the occurrence of coarse grained corundum and garnet within a randomly-oriented matrix made up of chlorite and margarite (Fig. 2f). The following characteristic assemblages are observed (Table 1): Crn + Grt + Chl + Zo + Mrg + Ilm (*Sau1*); Crn + Grt + Bt + Chl + Mrg ± St + Ilm (*Sau2*, *Sau2b*,

Table 2. *Selected mineral compositional data of the rocks that surround the ultramafic body. "maf" refers to the amphibolites. Electron microprobe analyses obtained by a wave-length dispersed SEK JEOL JSM-6310 under conditions of 5nA beam current and 15 kV voltage at Karl Franzens University of Graz. Mineral formulae and Fe_2O_3 contents were calculated with the computer program AX (*Holland *and* Powell, *1998). Mole fractions of end members are defined in the text. The analyses listed here are those used for the average* PT *calculations shown on Fig. 5 (in garnet, core compositions were used)*

(a)

Garnet											Biotite							Staurolite				
Sample	Sau11	Sau8	Sau8	Sau5	Sau5	Sau3	Sau2	Sau2	Sau9	Sau21	Sample	Sau11	Sau8	Sau8	Sau3	Sau5	Sau2	Sample	Sau11	Sau3	Sau5	Sau2
Zone	zone 1	zone 1	zone 1	zone 2	zone 2	zone 2	zone 3	zone 3	maf (zone 1)	maf (zone 2)	Type	zone 1	zone 1	zone 1	zone 2	zone 2	zone 3	Type	zone 1	zone 2	zone 2	zone 3
Site	*core*	*rim*	*core*	*rim*	*core*		*rim*	*core*			*Site*						*inc.*	*Site*		*inc.*		*inc.*
SiO_2	38.93	37.33	37.71	37.65	37.65	38.27	38.36	37.12	37.74	38.40	SiO_2	37.01	36.68	37.95	36.54	36.19	36.43	SiO_2	29.02	28.31	28.66	28.47
TiO_2	0.00	0.09	0.17	0.09	0.05	0.06	0.08	0.25	0.16	0.16	TiO_2	1.77	1.59	1.67	1.54	0.54	1.21	TiO_2	0.58	0.62	0.40	0.53
Al_2O_3	21.37	20.84	21.13	21.86	21.42	22.10	21.81	20.68	20.81	21.52	Al_2O_3	18.30	18.46	19.23	18.19	20.76	19.33	Al_2O_3	54.24	52.07	54.59	53.52
Fe_2O_3	0.00	0.14	0.00	1.01	1.40	0.54	1.22	0.65	1.22	1.42	Fe_2O_3	0.00	0.00	0.00	1.28	2.77	2.24	FeO	11.5	11.48	12.51	12.36
FeO	30.91	30.67	28.58	32.23	29.03	29.70	30.05	30.74	23.09	25.38	FeO	17.60	17.49	16.94	13.25	14.14	11.51	MnO	0.00	0.01	0.00	0.12
MnO	0.66	0.05	0.08	0.19	0.15	0.38	1.09	0.85	1.71	0.54	MnO	0.01	0.03	0.00	0.09	0.02	0.00	MgO	1.75	3.79	1.31	2.87
MgO	4.52	3.25	3.47	4.49	5.07	7.01	4.16	2.35	2.38	5.31	MgO	10.06	11.29	11.92	13.57	12.94	14.57	CaO	0.06	0.01	0.00	0.03
CaO	4.66	6.40	8.04	3.64	5.10	2.53	5.15	6.79	12.65	8.22	CaO	0.00	0.19	0.07	0.02	0.02	0.00	Na_2O	0.05	0.06	0.00	0.07
											Na_2O	0.28	0.24	0.21	0.33	0.36	0.50					
Total	101.1	98.8	99.2	101.2	99.9	100.6	101.9	99.4	99.8	101.0	K_2O	8.95	8.07	7.87	7.97	7.15	7.99	Total	98.5	96.4	97.5	98.0
Number of cations on the basis of 12 (O)											Total	94.0	93.8	92.8	94.0	95.9	94.9	Number of cations on the basis of 46 (O)				
Si	3.04	3.00	3.00	2.95	2.97	2.97	2.98	2.99	2.98	2.97								Si	7.94	7.90	7.90	7.83
Ti	0.00	0.01	0.01	0.01	0.00	0.00	0.01	0.02	0.01	0.01	Number of cations on the basis of 11 (O)							Ti	0.12	0.13	0.08	0.11
Al	1.97	1.98	1.98	2.02	1.99	2.02	1.99	1.96	1.94	1.96	Si	2.81	2.77	2.79	2.76	2.67	2.70	Al	17.50	17.12	17.74	17.36
Fe^{3+}	0.00	0.01	0.00	0.06	0.08	0.03	0.07	0.04	0.07	0.08	Ti	0.10	0.09	0.09	0.09	0.03	0.07	Fe^{2+}	2.89	2.67	2.88	2.84
Fe^{2+}	2.02	2.06	1.90	2.12	1.91	1.93	1.95	2.07	1.53	1.64	Al	1.64	1.65	1.67	1.61	1.81	1.69	Mn	0.00	0.00	0.00	0.03
Mn	0.04	0.00	0.01	0.01	0.01	0.03	0.07	0.06	0.12	0.04	Fe^{3+}	0.00	0.00	0.00	0.07	0.15	0.13	Mg	0.7	1.57	0.54	1.18
Mg	0.53	0.39	0.41	0.53	0.60	0.81	0.48	0.28	0.28	0.61	Fe^{2+}	1.12	1.11	1.04	0.84	0.87	0.71	Ca	0.02	0.00	0.00	0.01
Ca	0.39	0.55	0.69	0.31	0.43	0.21	0.43	0.59	1.07	0.68	Mn	0.00	0.00	0.00	0.01	0.00	0.00	Na	0.03	0.03	0.00	0.04
											Mg	1.14	1.27	1.31	1.53	1.42	1.61					
Total	7.99	8.00	8.00	8.00	7.99	8.00	7.98	8.00	8.00	7.99	Ca	0.00	0.02	0.01	0.00	0.00	0.00	Total	29.21	29.43	29.15	29.40
											Na	0.04	0.04	0.03	0.05	0.05	0.07					
											K	0.87	0.78	0.74	0.77	0.67	0.76	X_{Fe}	0.8	0.63	0.84	0.71
End-member molar fractions																						
X_{Alm}	0.68	0.69	0.63	0.71	0.65	0.65	0.67	0.69	0.51	0.55	Total	7.72	7.72	7.67	7.72	7.68	7.74					
X_{Py}	0.18	0.13	0.14	0.18	0.20	0.27	0.16	0.09	0.09	0.21												
X_{Sps}	0.01	0.00	0.00	0.00	0.00	0.01	0.02	0.02	0.04	0.01	X_{Fe}	0.50	0.47	0.44	0.35	0.38	0.31					
X_{Grs}	0.13	0.18	0.23	0.10	0.15	0.07	0.15	0.20	0.36	0.23												
X_{Fe}	0.79	0.84	0.82	0.80	0.76	0.70	0.80	0.88	0.85	0.73												

(*continued*)

Table 2 (*continued*)

(b)

Plagioclase				White micas							Chlorite				Amphibole			Zoisite	
Sample	Sau11	Sau8	Sau5	Sample	Sau11	Sau8	Sau5	Sau3	Sau2	Sau19	Sample	Sau2	Sau19	Sau21	Sample	Sau9	Sau21	Sau9	Sau21
Zone	zone 1	zone 1	zone 2	Zone	Zone 1	zone 1	zone 2	zone 2	zone 3	zone 3	Zone	zone 3	zone 3	maf (zone 2)	Zone	maf (zone 1)	maf (zone 2)	maf (zone 1)	maf (zone 2)
				Mica	*mu*	*mu*	*mu*	*prg*	*mrg*	*mrg*									
SiO_2	61.08	62.90	62.91	SiO_2	49.59	48.20	46.93	44.74	30.95	28.96	SiO_2	26.69	26.26	26.92	SiO_2	46.62	40.80	38.85	38.31
TiO_2	0.00	0.00	0.00	TiO_2	0.92	0.79	0.85	0.20	0.16	0.07	TiO_2	0.04	0.07	0.08	TiO_2	0.44	0.59	0.08	0.00
Al_2O_3	24.73	22.88	22.78	Al_2O_3	31.96	34.84	35.91	40.21	49.58	47.80	Al_2O_3	20.96	22.18	22.65	Al_2O_3	10.38	18.15	31.14	28.96
Fe_2O_3	0.01	0.10	0.10	Fe_2O_3	0.00	1.05	0.00	0.00	0.00	0.56	Fe_2O_3	0.00	0.03	0.02	Cr_2O_3	0.00	0.16	0.00	0.00
FeO	0.00	0.00	0.00	FeO	1.17	0.41	0.95	0.33	0.42	0.22	FeO	23.51	14.77	15.02	Fe_2O_3	0.00	5.20	0.00	2.84
MnO	0.04	0.01	0.02	MnO	0.00	0.05	0.00	0.13	0.00	0.00	MnO	0.12	0.04	0.09	FeO	12.93	7.46	1.79	2.46
MgO	0.00	0.00	0.00	MgO	1.78	1.34	0.51	0.25	0.64	0.51	MgO	14.21	21.73	22.02	MnO	0.07	0.19	0.18	0.00
CaO	6.71	4.75	4.73	CaO	0.00	0.00	0.03	1.74	12.49	10.87	CaO	0.04	0.07	0.00	MgO	11.66	11.43	0.16	0.14
Na_2O	7.78	8.28	8.31	Na_2O	1.51	1.01	1.58	6.03	1.19	1.33	Na_2O	0.06	0.02	0.00	CaO	12.17	11.03	25.29	23.01
K_2O	0.06	0.11	0.11	K_2O	8.87	7.71	7.96	0.62	0.01	0.00	K_2O	0.07	0.00	0.00	Na_2O	1.29	1.83	0.03	1.77
															K_2O	0.21	0.28	0.00	0.00
Total	100.4	99.0	99.0	Total	95.8	95.4	94.7	94.3	95.4	90.3	Total	85.7	85.2	86.8	Total	95.8	97.1	97.5	97.5
Number of cations on the basis of 8 (O)				Number of cations on the basis of 11 (O)							Number of cations on the basis of 14 (O)				Basis of 23 (O)			Basis of 12.5 (O)	
Si	2.70	2.80	2.81	Si	3.25	3.14	3.09	2.90	2.06	2.03	Si	2.84	2.69	2.70	Si	6.92	5.95	3.00	3.00
Ti	0.00	0.00	0.00	Ti	0.05	0.04	0.04	0.01	0.01	0.00	Ti	0.00	0.01	0.01	Ti	0.05	0.07	0.01	0.00
Al	1.29	1.20	1.20	Al	2.47	2.68	2.79	3.07	3.88	3.95	Al	2.63	2.68	2.68	Al	1.82	3.12	2.84	2.67
Fe^{3+}	0.00	0.00	0.00	Fe^{3+}	0.00	0.05	0.00	0.00	0.00	0.03	Fe^{3+}	0.00	0.00	0.00	Cr	0.00	0.02	0.00	0.00
Fe^{2+}	0.00	0.00	0.00	Fe^{2+}	0.06	0.02	0.05	0.02	0.02	0.01	Fe^{2+}	2.09	1.27	1.26	Fe^{3+}	0.00	0.57	0.00	0.17
Mn	0.00	0.00	0.00	Mn	0.00	0.00	0.00	0.01	0.00	0.00	Mn	0.01	0.00	0.01	Fe^{2+}	1.61	0.91	0.12	0.16
Mg	0.00	0.00	0.00	Mg	0.17	0.13	0.05	0.02	0.06	0.05	Mg	2.25	3.32	3.30	Mn	0.01	0.02	0.01	0.00
Ca	0.32	0.23	0.23	Ca	0.00	0.00	0.00	0.12	0.89	0.82	Ca	0.00	0.01	0.00	Mg	2.58	2.48	0.02	0.02
Na	0.67	0.72	0.72	Na	0.19	0.13	0.20	0.76	0.15	0.18	Na	0.01	0.00	0.00	Ca	1.94	1.72	2.09	1.93
K	0.00	0.01	0.01	K	0.74	0.64	0.67	0.05	0.00	0.00	K	0.01	0.00	0.00	Na	0.37	0.52	0.01	0.27
															K	0.04	0.05	0.00	0.00
Total	4.98	4.96	4.96	Total	6.93	6.84	6.90	6.96	7.07	7.07	Total	9.85	9.97	9.95	Total	15.33	15.42	8.08	8.22
X_{An}	0.32	0.24	0.24	X_{ms}	0.80	0.83	0.77	0.06	0.00	0.00	X_{Fe}	0.48	0.28	0.28					
				X_{mrg}	0.00	0.00	0.00	0.13	0.85	0.82									
				X_{prg}	0.20	0.17	0.23	0.81	0.15	0.18									

Sau2c, *Sau15a*) and: Crn + Chl + Mrg + Ilm (*Sau19*). The second of these three assemblages is the least retrogressed. In this assemblage, garnets are euhedral with a diameter of up to 4 centimeters and are chemically homogeneous, showing only a narrow rim with elevated X_{Fe} (X_{Fe} in the core = 0.78–0.81 and X_{Fe} = 0.88–0.90 in the rims). The calcium content ($X_{Grs} = Ca/(Ca + Mn + Mg + Ca) = 0.19–0.21$) is higher than that obtained in the mica-schists and the $X_{Sps} = Mn/(Ca + Mn + Mg + Ca)$ is always lower than 0.01. Primary chlorite (Chl1) in the matrix, (Fig. 2f, g) has higher iron contents ($X_{Fe} = 0.47–0.53$) in the assemblage of *Sau2* than in the assemblage of *Sau19*. Staurolites in the matrix are usually replaced by a second generation of chlorite (Chl2) (Fig 2f). Margarite crystals are up to 1 cm long and have sodium contents of $(Na/(Ca + Na) = 0.15$ to 0.18. Small aggregates of biotite, margarite and staurolite appear as inclusions inside individual corundum crystals (Figs. 2g, h). Staurolite inclusions inside corundum have an iron magnesium ratio of $X_{Fe} = 0.71$. Biotite in equilibrium with staurolite inside the corundum has an X_{Fe} of 0.31 (Fig. 2h). Interestingly, these phases are considerably more Mg rich than the rocks in zone 1.

Zone 4: Ultramafic rocks

The rocks in the ultramafic body have a granoblastic texture without any preferred orientation. In the inner part of the body the typical assemblage is olivine + talc + tremolite. Chlorite can be present in a small proportion as the only aluminum-bearing phase. Secondary serpentine appears associated with olivine as fibrous aggregates. Dark brown spinel grains are also present. Typically these occur as inclusions in randomly-oriented tremolite fibers that are up to several centimeters long. In the outer part of the ultramafic body the dominant assemblage is talc + tremolite. The abundance of talc gives the rock a white appearance in hand specimen. In some samples olivine appears as a relic mineral phase surrounded by fine grained talc which suggests that olivine has reacted to form talc in the outermost part of the ultramafic body, close to the contact with the aluminous country rocks.

Geochemical changes

Bulk compositional variation across the mapped zonation is the key to the interpretation of the formation process. We therefore discuss here the bulk compositions of the four most important zones. Whole rock analyses of the rocks from the four zones are shown in Table 3 and are illustrated on Figs. 3, 4. All chemical changes must be seen in view of the ultramafic body that forms the centre of the zonation. The analysed ultramafic body (zone 4) is made up of 50% SiO_2, 27% MgO, 7% FeO and 4% CaO. Although *Schmerold* (1988) has suggested that most of the Saualm ultramafic bodies have a lherzolitic composition, this bulk composition differs from lherzolites or harzburgites as defined by *Wilson* (1989). In the outer part of the ultramafic body the rocks appear to be somewhat enriched in silica as indicated by the silica-consuming breakdown of olivine to form talc in the outer parts of the body.

Rocks in the far field mica-schist (zone 1) have bulk compositions of typical alumina-rich metapelites (Table 3, Fig. 3). Compared to metapelite analyses averaged from elsewhere in the Sau-Koralm region (see Table caption 3), the sample

Table 3. *Whole rock analyses of the rock types from the different zones. The elements Be, Zn, As, Mo, Ag In and Sb were also analysed but were below detection limits in most samples. The "average host" analysis is a mean mica-schist composition from sample* Sau7, *the whole rock analyses published by* Stüwe *and* Powell *(1995)*

Zone	zone-1	zone-1	zone-2		zone-3	zone-4
Rock type	average host	micaschist	metasomatised zone		corund. rocks	ultramafic
Sample		Sau-7	Sau-5	Sau-22	Sau-2	Sau-6
Major elements (wt %)						
SiO_2	63.91	54.92	51.80	52.63	30.36	50.68
Al_2O_3	15.67	12.42	25.02	24.38	37.56	1.71
Fe_2O_3	5.76	5.66	9.73	9.32	14.09	6.91
MnO	0.18	0.65	0.13	0.11	0.16	0.14
MgO	2.29	2.00	2.05	2.42	3.69	27.39
CaO	2.98	11.16	1.52	1.80	8.55	4.41
Na_2O	1.88	0.76	1.40	1.89	0.49	0.07
K_2O	2.81	2.25	3.64	2.79	0.62	0.04
TiO_2	0.65	0.52	1.05	1.00	1.43	0.04
P_2O_5	0.13	0.09	0.12	0.14	0.21	0.02
LOI	n.d.	8.61	3.11	2.48	2.07	7.57
Total	96.26	99.05	99.56	98.96	99.23	98.98
Trace elements (XRF fusion pellet ACTLABS Job No. A04-0084, ppm)						
Ba		357	570	407	93	17
Sr		245	200	229	988	32
Y		24	31	34	68	5
Sc		12	23	24	43	9
Zr		95	134	141	158	5
V		90	141	146	162	42
Trace elements (ICPMS Lithochem ACTLABS Job No. A04-0084, ppm)						
V		85	128	137	154	51
Cr		90	120	128	177	1880
Co		14	14	19	80	96
Ni		70	27	56	64	1220
Cu		56	17	13	11	15
Ga		16	30	31	35	3
Ge		1	2	2	2	3
Rb		93	158	111	40	2
Sr		230	186	222	964	31
Y		25	30	35	71	5
Zr		100	142	141	157	6
Nb		15	27	22	30	7
Sn		2	5	4	10	4
Cs		3.1	4.4	3.4	4.4	0
Ba		347	540	408	91	15
La		25.3	21.6	47.7	101	3.1
Ce		46.7	47.9	103	198	4.7
Pr		6.02	5.08	11.2	22.4	0.45

n.d. not determined

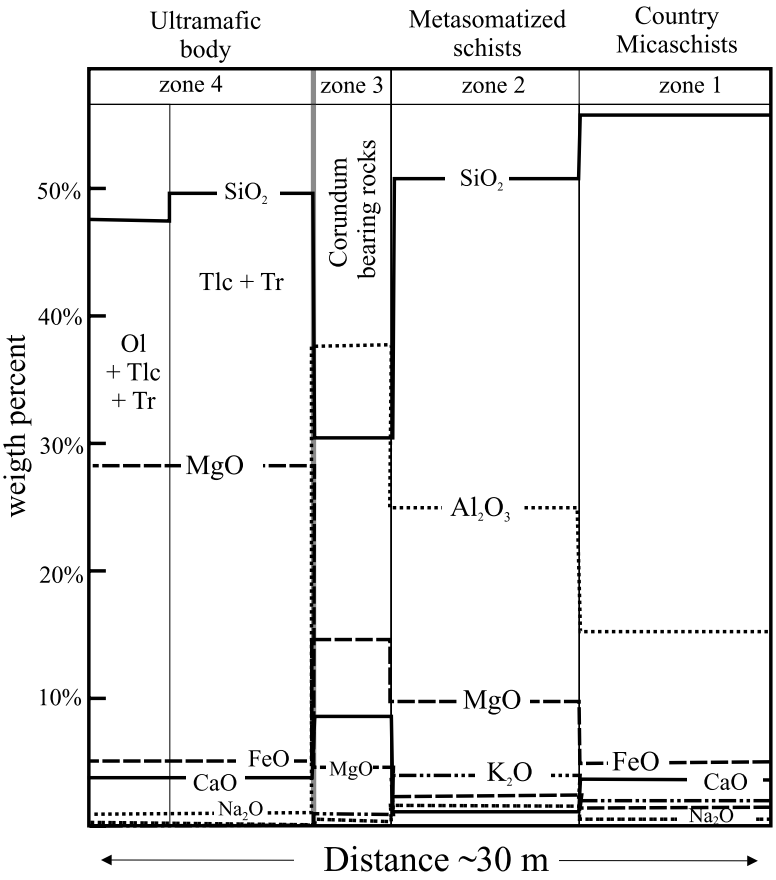

Fig. 3. Schematic diagram showing the changes of concentration of elements across the transect using the bulk rock analyses from Table 3. The contact of the ultramafic body is shown by the shaded bar. The location of initial contact is clearly marked by a discontinuity in the Al_2O_3 between the tremolite-talc zone and the corundum zone. This discontinuity match in other localities (*Sandford*, 1982) with a discontinuity in the Cr/Ti rations

analysed here (*Sau7*) has exceptionally high CaO content (11 wt%) and low SiO_2 content (55 wt%), indicating that this sample may not have been sampled far enough removed from the alteration zone as to represent the unaltered pelite. However, all other components are consistent with a number of other analyses

Fig. 4. Isocon plots illustrating mass changes in the metasomatized zones 2 and 3. The horizontal axis shows element concentration (in ppm) in the average mica-schists (1st column on Table 3), the vertical axes show element concentrations (in ppm) in the samples indicated in the insets. Diagrams at left are for major elements. Diagrams at right are for trace elements. All concentrations are shown in ppm. For trace elements that were analysed with two methods (V, Sr, Ba, Zr and Y) the average was taken. Dashed lines show isocons with a slope of 1. Continuous lines show best fit isocons using the method of *Baumgartner* and *Olsen* (1995). Slopes (intercepts on the doubly logarithmic plot) are indicated along the isocon

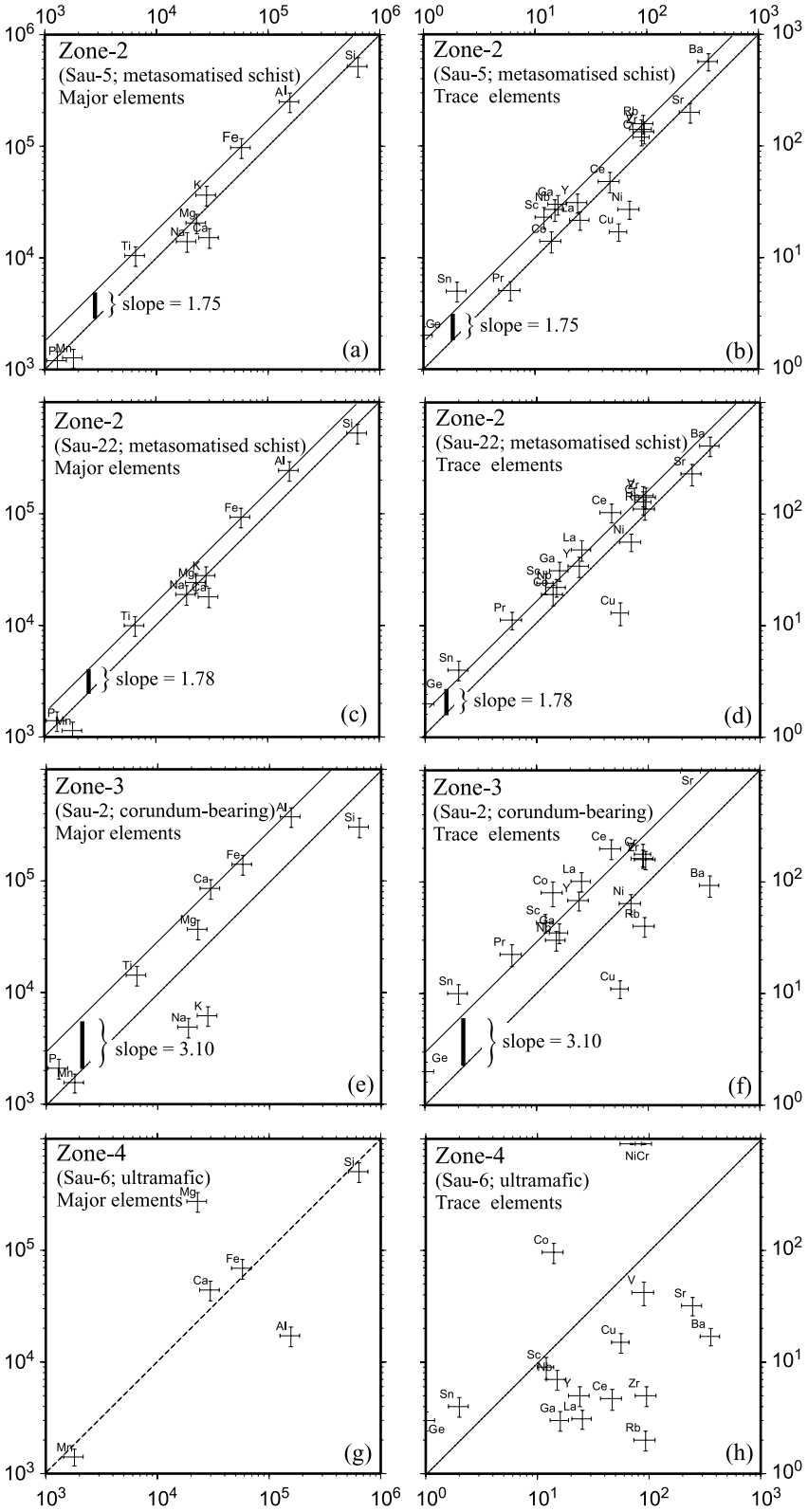
Zone-2
(Sau-5; metasomatised schist)
Major elements
slope = 1.75
(a)
Zone-2
(Sau-5; metasomatised schist)
Trace elements
slope = 1.75
(b)
Zone-2
(Sau-22; metasomatised schist)
Major elements
slope = 1.78
(c)
Zone-2
(Sau-22; metasomatised schist)
Trace elements
slope = 1.78
(d)
Zone-3
(Sau-2; corundum-bearing)
Major elements
slope = 3.10
(e)
Zone-3
(Sau-2; corundum-bearing)
Trace elements
slope = 3.10
(f)
Zone-4
(Sau-6; ultramafic)
Major elements
(g)
Zone-4
(Sau-6; ultramafic)
Trace elements
NiCr
(h)

from the region. The exceptionally high CaO content is not accompanied by high Na_2O and is therefore unlikely to be related to plagioclase porphyroblasts. However, marble bands are widespread through the region and interfinger with the metapelites on a centimetre scale. It is suggested that this high CaO content is related to calcite veining in the analysed sample.

In contact zones 2 and 3 a successive silica depletion from 52 wt% SiO_2 (in zone 1) to about 30 wt% SiO_2 in zone 3 can be observed. This successive silica depletion with proximity to the ultramafic body is accompanied by a successive enrichment of Al_2O_3, FeO and MgO. This is also reflected by equivalent enrichments in MnO, TiO_2, and P_2O_5. All these elements give the impression that their enrichment relative to the undisturbed precursor may be due to the extraction of silica. However, this trend cannot be observed in the alkalis which show no obvious trends. CaO contents are below 2 wt% in zone 2 but above 8% in zone 3 (compared to 4 wt% in the ultramafic rocks and about 3 wt% in the mica-schists). Na_2O contents are also below 2 wt% in zone 2 but decrease to less than 1 wt% in zone 3 and K_2O contents are around 3 wt% in zone 2 but below 1 wt% in zone 3. These trends are apparently related to the successive replacement of plagioclase and muscovite by paragonite, chlorite and margarite with proximity to the contact to the ultramafic body. Margarite contains more CaO but less Na_2O than plagioclase so that substantial proportions of margarite replacing plagioclase (as are present in zone 3) will cause elevated CaO, but depleted Na_2O contents and replacement of muscovite by margarite and paragonite can explain the depletion in K_2O. Conversely, the abundant presence of chlorite in zone 3 (being free of both CaO and Na_2O) can explain the depletion in Na_2O but not the enrichment of CaO. In summary, the relative abundances of white micas and chlorite replacing muscovite will determine the details of the concentration changes of the alkalis in zones 2 and 3. Nevertheless, the relative abundance of elements in the altered rocks and the protolith gives only an idea about the depletion or enrichment of elements relative to the protolith. It does not show the absolute gain and loss of mass due to metasomatism or mobility of some elements.

Mass changes during metasomatism

The gain or loss of mass or volume and the relative depletion of mobile elements can elegantly be shown using the isocon plot (*Grant*, 1986). This diagram is a graphical solution of *Gresens* equation (*Gresen*, 1967) for metasomatism and has been widely applied to the discussion of mass changes in alteration zones and shear zones (*Hippert*, 1998; *Robl* et al., 2004). In the isocon plot the element concentrations of the protolith (the least altered rock) are plotted against the element concentrations of the altered rocks. An ''isocon'' is a line of constant mass on this diagram. Immobile elements plot on a straight line passing through the origin of the diagram. However, the slope of this line need not to be 1. A shallower or steeper slope indicates dilution or concentration of immobile elements in the altered rock relative to the protolith, respectively.

Isocon plots for the metasomatized zones 2 and 3 are shown on Figs. 4a–f. For all plots on Fig. 4 we used a protolith composition of the regional mica-schists that was averaged from 6 bulk rock analyses for the mica-schist published by different authors (see Table 3). Figure 4 is refined from a ''normal'' isocon plot

(*Grant*, 1986) by using a logarithmic scale, a 10% relative error for each element and a least square approach for fitting isocons (*Baumgartner* and *Olsen*, 1995). Note that because of the logarithmic scale the error bars appear asymmetric. Note also that all isocons have a slope of 1 on a log – log plot. Different slopes of isocons on a linear plot appear as parallel lines offset from the diagonal on the logarithmic plots. In Figs. 4g, h the regional mica-schists are compared with the ultramafic body. However, note that these figures are strictly not isocon plots as the ultramafic rocks did not form by metasomatic alteration from the mica-schist protolith.

In zone 2 the best fit isocon has a slope of 1.75 indicating a mass loss of about 43% from the original rock. The mass loss as derived from the slope of the isocon is the same for both the trace elements and the major elements and very similar between the two analysed samples (it is 75% for sample *Sau5* and 78% for sample *Sau22*) (Figs. 4a–d). The isocon is defined by the majority of the analysed trace elements as well as the major elements FeO, Al_2O_3 and TiO_2. From this isocon, the elements showing the most significant changes are SiO_2, Na_2O, K_2O and CaO. These elements show significant depletion and were apparently mobile during the mass loss. MnO also shows a significant depletion but because of the low absolute values this may be related to the depletion of oxides and will not be interpreted here.

In zone 3 the best fit isocon has a slope of 3.10 indicating a mass loss of some 68% from the original rock (Figs. 4e, f). The isocon is defined by the same elements as in zone 2 but CaO also fits the isocon well. Significant depletion of mobile elements occurs for SiO_2, Na_2O and K_2O. The depletion of these three elements is about three times that in zone 2. The fact that CaO is significantly depleted in zone 2 but appears on the isocon in zone 3 suggests that the apparent depletion in zone 2 may be due to a sampling problem. It also suggests that most of the mass loss is related to breakdown of muscovite to form margarite. Plagioclase breakdown to margarite can explain depletion in Na_2O.

In summary, the comparison of bulk compositions on isocon plots suggests that the elements Al_2O_3, FeO, TiO_2 and to some extent MgO remained largely immobile during the metasomatic process This reduces the process of metasomatism to a process involving successive depletion of SiO_2, Na_2O and K_2O in zone 2 and zone 3 and possibly an additional massive depletion of CaO in zone 2 only.

Formation conditions

The strong variation of bulk compositions across several zones suggests that the process of corundum formation is a metasomatic alteration process that occurred during a regional metamorphic event. The fact that the synmetamorphic fabric is partly obliterated by the coarse grained metasomatic assemblages indicates that the zonation formed during or after the last pervasive deformation event of the region. Ultramafic rocks in the Saualpe are known to have intruded in the Variscan and Permian (*Thöni* and *Jagoutz*, 1992). They have subsequently been deformed and metamorphosed together with the surrounding sequence during the Eo-Alpine orogenic cycle. We therefore assume that the metasomatic process

occurred during the Eo-Alpine metamorphic cycle. Eo-Alpine metamorphism of rocks north of the study area occurred at around 20 kbar and 680 °C and at around 575 °C and 7 kbar in the later stages of this event (*Thöni* and *Miller*, 1996). In contrast, *Habler* and *Thöni* (2001) showed that older signatures of a Permian metamorphic event around 600 °C and 4 kbar may also be extracted from the eclogite facies rocks. Formation conditions in the overlying Plankogel series (in which the Lölling occurrence is located) are less well constrained, although *Tenczer* and *Stüwe* (2003) and *Gregurek* et al. (1997) have documented conditions around 600 °C and 10 kbar from elsewhere within the Plankogel series. In view of these ill-constrained formation conditions for the Plankogel series and the fact that we will later discuss the metasomatic process in terms of isobaric-isothermal phase diagrams it is important to constrain the formation conditions as closely as possible.

PT conditions during formation

The regional metamorphic conditions during the metasomatic process at the Lölling area are constrained by the occurrence of the assemblage olivine + talc in the ultramafic body. This assemblage implies metamorphic peak temperatures above the reaction Atg = Fo + Tlc + H_2O in the system MgO–SiO_2–H_2O (MSH), where all the primary serpentine is consumed to form olivine and talc. It is further constrained to be below the reaction Fo + Tlc = En + H_2O in the same system (Fig. 5a). Additionally, the occurrence of kyanite in the mica-schists suggests that equilibrium was reached at pressures above the sillimanite = kyanite reaction (Fig. 5a). These limits on the formation conditions are confirmed by *PT* estimates using THERMOCALC (*Powell* and *Holland*, 1988). Average *PT* calculations were performed using mineral end member activities calculated from microprobe analyses (using the program AX of *Holland* and *Powell*, 1998). Six assemblages were selected across the zonation to provide independent estimates from different bulk compositions. Results are shown in Fig. 5a and compared with selected CMSH and MSH reactions. The results show that highest temperatures and standard deviations are given by samples that are quartz-free (*Sau3* and *Sau2* – see Tables 1 and 2 for listing of the used parageneses). It is suggested that this is because of incomplete equilibration during metasomatic alteration. Results for the four samples *Sau5*, *Sau8*, *Sau9* and *Sau11* are consistent with the qualitative estimates for CMSH assemblages in the ultramafic body (shaded region). They indicate formation conditions in the range between 6–9 kbar and 570–650 °C.

In order to provide more refined estimates of the formation conditions, thermodynamic pseudosections were calculated for the metapelites of zone 1 and the corundum-bearing rocks of zone 3, using bulk compositions for the samples *Sau11* and *Sau2*, *Sau2b* and *Sau2c*, respectively. The pseudosections were calculated in the system Na_2O–CaO–K_2O–FeO–MgO–Al_2O_3–SiO_2–H_2O (NCKFMASH). Because it is non-trivial to reduce the whole rock analyses shown in Table 3 to this 8 component subsystem (in particular in view of the partially ill-equilibrated nature of the peak parageneses), the bulk compositions for these pseudosections were obtained by point counting mineral modes and converting those to oxide weight percent normalized to one oxide as required for input in THERMOCALC

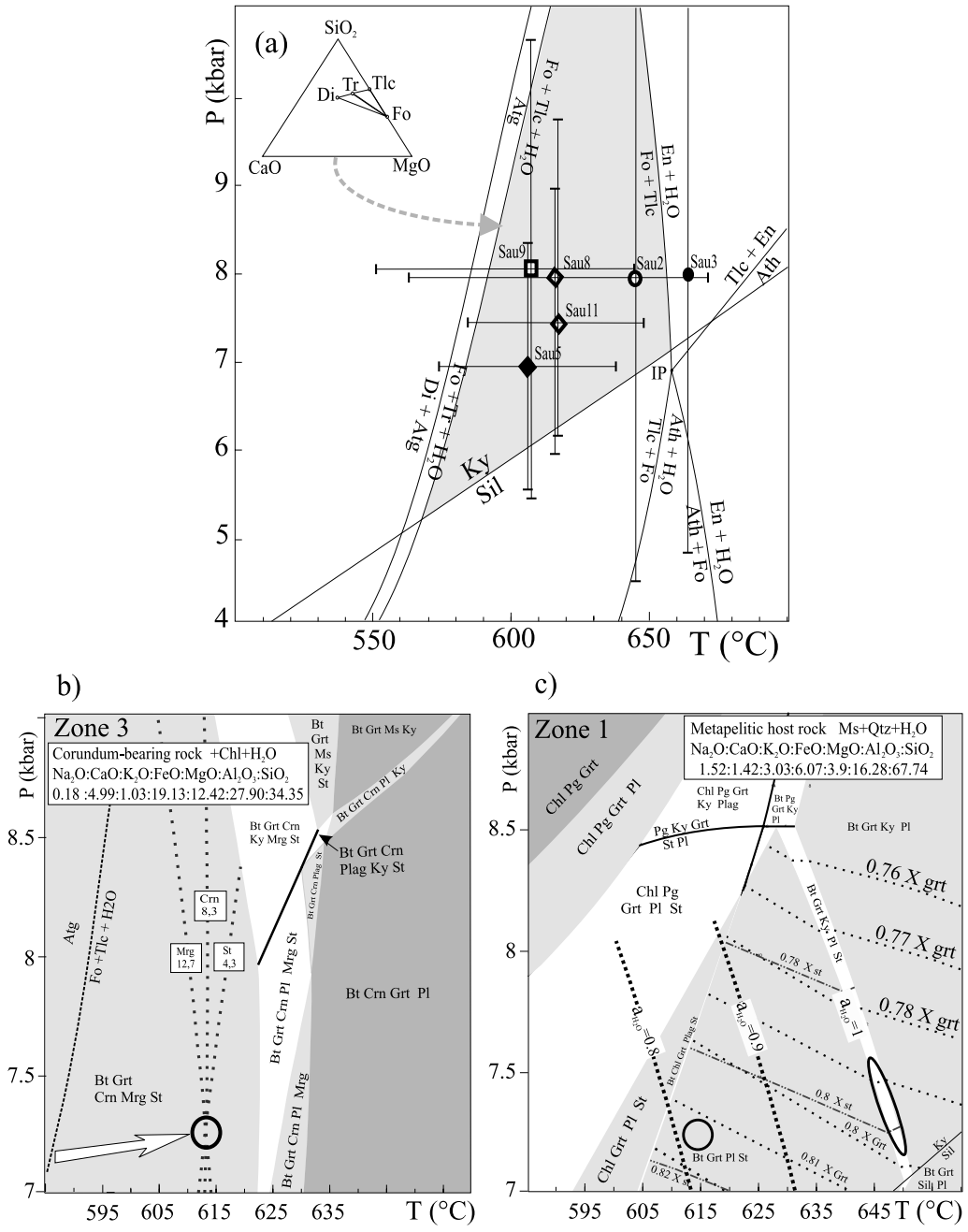

Fig. 5. **a** Partial petrogenetic grid for the system MgO–SiO_2–H_2O (plus the Ca–MSH univariant reaction $Di + Atg = Fo + Tr + H_2O$) showing average *PT* calculations for six selected samples in the study area (assemblages used for the average *PT* calculations are labelled with "PT" in Table 1 and 2). Shaded area shows the stability range of the ultramafic assemblages. **b** Pseudosection for zone 3 (sample *Sau2*). The open circle shows the estimated peak conditions from modal proportions. Dotted lines are labelled modal contours. White arrow: Prograde path proposed for the study area. Dashed line: Reaction for the subsystem MSH. **c** Pseudosection for zone 1 (sample *Sau11*). The thick ellipse shows the stability range of the peak parageneses in zone 1 for water activity of 1. This field shifts to lower temperatures for a more realistic water activity below 1. This is shown for the kyanite-out contour at $a_{H_2O} = 0.9$ and $a_{H_2O} = 0.8$ (thick dotted lines). Divariant fields are shown white; trivariant fields are light shaded; quadrivariant fields are shaded dark

Table 4. *Data used to calculate the bulk compositions used for the pseudosections of Fig. 3b and c.* ***a*** *and* ***b*** *Point counting results of samples* Sau2 *and* Sau11*, the mean compositions of the phases (from Table 2) and the molar volumes used. Abbreviations for the compositional parameters are those used by THERMOCALC.* $Xst = Xgrt = Xchl = Xbt = Xms = Fe/(Fe+Mg)$; $Y(chl) = AlIV/2$; $Ybt = (Al,\ M1)$; $Yms = (Al,\ M2A)$; $Nms = Na/(Na+K)$; $Nmrg = Na/(Na+Ca)$; $Zgrt = Ca/(Fe+Mg+Ca)$; $Xan = Ca/(Ca+Na)$. ***c*** *Bulk compositions derived from the data in* ***a*** *and* ***b*** *using THERMOCALC. The "ratio" line shows the elative depletion/enrichment for each component.* ***d*** *Data from* ***c*** *in graphic form*

(a)

Sau2	Mode	Composition	Volume ($Jbar^{-1}$)
Garnet	27	Xgrt = 0.88; Zgrt = 0.2	11.5
Staurolite	4.3	Xst = 0.71	44.8
Chlorite	32.7	Xchl = 0.48; Ychl = 0.7	21.0
Biotite	15	Xbt = 0.31; Ybt = 0.39	15.0
Margarite	12.7	Nmrg = 0.21	13.0
Corundum	8.3		2.6

(b)

Sau11	Mode	Composition	Volume ($Jbar^{-1}$)
Garnet	6.1	Xgrt = 0.79; Zgrt = 0.13	11.5
Staurolite	3.25	Xst = 0.8	48.8
Chlorite	0.65	Xchl = 0.4; Ychl = 0.6	4
Biotite	9.6	Xbt = 0.49; Ybt = 0.45	15
Muscovite	32.7	Xms = 0.27; Nms = 0.21; Yms = 0.7	14
Kyanite	4.5		44.8
Plagioclase	14.1	Xan = 0.32	11.35
Quartz	28.2		2.27
Rutile	0.4		2.1
Ilmenite	0.65		1.3

(c)

	Na_2O	CaO	K_2O	FeO	MgO	Al_2O_3	SiO_2
Sau11	1.52	1.42	3.03	6.07	3.94	16.28	67.74
Sau2	0.18	4.99	1.03	19.13	12.42	27.90	34.35
Ratio	*−88%*	*253%*	*−66%*	*215%*	*215%*	*71%*	*−49%*
Tr–Tlc	–	5.15	–	1.45	39.38	1.93	52.08
Tr–Tlc–Ol	–	5.09	–	3.34	47.33	1.91	42.33
Ratio					*19%*		*−19%*

(d)

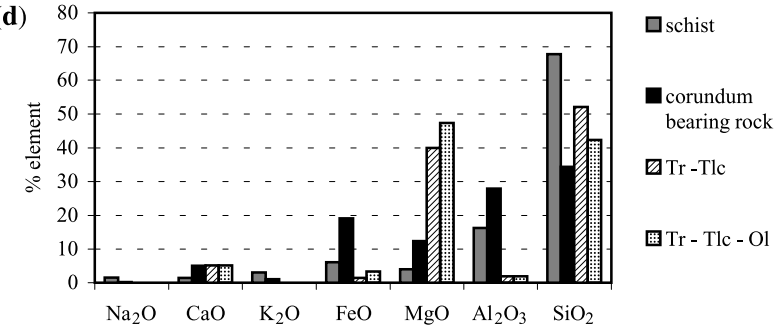

(Table 4) (e.g. *Stüwe* and *Powell*, 1995). More than 1000 points were counted in each of three thin sections for each sample (averaged from samples *Sau2*, *Sau2b* and *Sau2c* for the corundum-bearing rock of zone 3) and compositional data for minerals with solid solutions were estimated from microprobe analyses (Table 2). The molar volumes, used mineral compositions and modal results are listed in Table 4. The two bulk compositions are recalculated to hundred percent in terms of Na_2O, CaO, K_2O, FeO, MgO, Al_2O_3 and SiO_2 and are shown in Table 4c.

For zone 3 the coarse-grained peak assemblage of the selected sample *Sau2* (Bt–Chl–Grt–Crn–Mrg–St; Table 1) is trivariant in the system NCKFMASH and occupies a large field on the low temperature side of the pseudosection below about 620 °C in the pressure range estimated above (Fig. 5b). Above 620 °C plagioclase becomes stable, which was not found in the corundum-bearing rocks. Further constraints within this trivariant field can be obtained by intersections of mineral mode contours. Volumetric mode contours for margarite, corundum and staurolite intersect at precisely 615 °C and 7.2 kbar which is also consistent with the antigorite breakdown discussed above. Intersections of lines of constant composition (isopleths) are less useful, as isopleth contours are parallel to the pressure axis in this diagram. This explains why the average *PT* calculations have large errors and they provide no further detail.

For zone 1 we selected sample *Sau11* with the peak assemblage Bt–Grt–Ky–Pl–Ms–St–Qtz because it is practically free of retrograde overprint (Table 1). The peak assemblage of the metapelite sample *Sau11* is divariant in NCKFMASH and is stable within a narrow field around 650 °C at 7.2 kbar on the relevant pseudosection (Fig. 5c). We suggest that the difference in temperature estimates from the two pseudosections is caused by the fact that both were constructed for a water activity of 1. For zone 3 a water activity of 1 may be appropriate as we will show below that this zone formed due to infiltration-metasomatism by fluids liberated during prograde dehydration of the adjoining serpentinite. However, the regional metapelites of zone 1 probably formed at a water activity below 1 (*Tenczer* and *Stüwe*, 2003). The regional metapelites are known to have been extremely dry during Eo-Alpine metamorphism (e.g. *Stüwe* and *Powell*, 1995; *Habler* and *Thöni*, 2001; *Tenczer* and *Stüwe*, 2003) It is for that reason that earlier metamorphic assemblages (e.g. of Permian age) are partially preserved in the Saualpe (*Habler* and *Thöni*, 2001). Decreasing the water activity in the pseudosection for the metapelite (Fig. 5c) causes a rapid shift of the kyanite-out contour to lower temperatures (thick dashed lines in Fig. 5c). At $a_{H_2O} = 0.8$ the peak conditions for the metapelite precisely match those obtained for the corundum-bearing rock in Fig. 5b at $a_{H_2O} = 1$. Therefore we interpret a water activity of 0.8 as relevant for the metapelites in zone 1 and suggest *PT* conditions around 615 °C and 7.2 kbar as the appropriate formation conditions during metasomatism. This water activity is consistent with that suggested by *Tenczer* and *Stüwe* (2003) for the region.

Thermodynamic model and driving mechanism

The strong chemical zoning around the Lölling ultramafic body indicates that it is likely to have formed due to metasomatism. Metasomatic processes may occur by

diffusive exchange between zones of different bulk composition (''diffusion-metasomatism'') or by fluid infiltration from an external source (''infiltration-metasomatism''). Diffusion metasomatism is driven by chemical potential gradients and is typically efficient over length scales of the order of decimetres at most. Mass exchange over larger distances (as observed here) is difficult to explain with chemical potential gradients. In a fluid saturated environment it is theoretically possible and could possibly be inferred from a concentric metasomatic zoning. However, outcrop conditions at Lölling are too sparse to infer the symmetry of the zonation (the zoning shown in Fig. 1b is schematic) and we suggest here that the process is an infiltration metasomatic process. Within this interpretation, chemical potential is a dependent variable during the infiltration process and the formation process can be interpreted using equilibrium phase diagrams with pressure, temperature and chemical concentrations as the independent variables. However, we emphasize that chemical potential gradients still exist across the zonation (see also *Sanford*, 1982) – they simply cannot be made responsible as a driving mechanism.

The hypothesis that the corundum-bearing parageneses were formed by a metasomatic process involving SiO_2 and alkalis (in particular Na_2O and K_2O) from the metapelitic hosts was tested using an isothermal – isobaric $X_{Na_2O}-X_{SiO_2}$ pseudosection in the system NCKFMASH-TiO_2 (Fig. 6) (Neither T-X_{SiO_2} nor T-X_{MgO} pseudosections predicted any of the observed assemblages). The $X_{Na_2O}-X_{SiO_2}$ pseudosection is calculated for the bulk composition of the metapelites of zone 1 at the inferred peak *PT* conditions of 615 °C and 7.2 kbar (sample *Sau11*, Fig. 5c). The considered phases are: Grt, St, Pl, Bt, Ms, Mrg, Chl, Pg, Ky, Qtz, Ilm, Rt, Ctd, Neph, Zo, Spl, Crn and H_2O. In comparison to Fig. 5c we have added TiO_2 into the bulk composition used for the $X_{Na_2O}-X_{SiO_2}$ section for extra accuracy and because of the observed relationships between titanium oxides (Table 1). From the modal estimates of Table 4, 3% of TiO_2 was added to the bulk composition and recalculated to 100%. The ratio of the components CaO, FeO, MgO and Al_2O_3 shown in Fig. 6 is identical to that of Fig. 5c. The fractional contents of Na_2O and SiO_2 are defined as: $X_{Na_2O} = Na_2O/(CaO + K_2O + FeO + MgO + Al_2O_3 + TiO_2)$ and $X_{SiO_2} = SiO_2/(CaO + K_2O + FeO + MgO + Al_2O_3 + TiO_2)$. The inferred metasomatic change in K_2O is difficult to portray: In a two-dimensional X–X pseudosection it is not possible to illustrate the variation of more than two components simultaneously. We have therefore fixed the K_2O content of *Sau11* to a value high enough to form biotite in the corundum-bearing rocks of zone 3, but low enough to still have muscovite in all silica saturated parageneses at the inferred formation conditions of 615 °C and 7.2 kbar (Fig. 6). This value is between the K_2O content of *Sau11* and *Sau2*. As THERMOCALC does not allow a straightforward calculation of this diagram, the $X_{Na_2O}-X_{SiO_2}$ pseudosection was constructed by calculation of up to one hundred T-X_{Na_2O} diagrams for each X_{SiO_2}. Figure 6 shows this $X_{Na_2O}-X_{SiO_2}$ pseudosection in the range of $0 < X_{Na_2O} < 0.05$ (i.e. zero to 4.76% Na_2O content) and $0.3 < X_{SiO_2} < 0.9$ (i.e. $23\% < SiO_2 < 47.3\%$ content).

Figure 6 shows that both the peak parageneses of zone 1 and zone 3 are found on this diagram. In more general terms, the diagram includes both quartz-present and quartz-absent assemblages. Above a silica content of $X_{SiO_2} > 0.8$ all fields are quartz saturated and field boundaries are therefore straight lines parallel to the silica

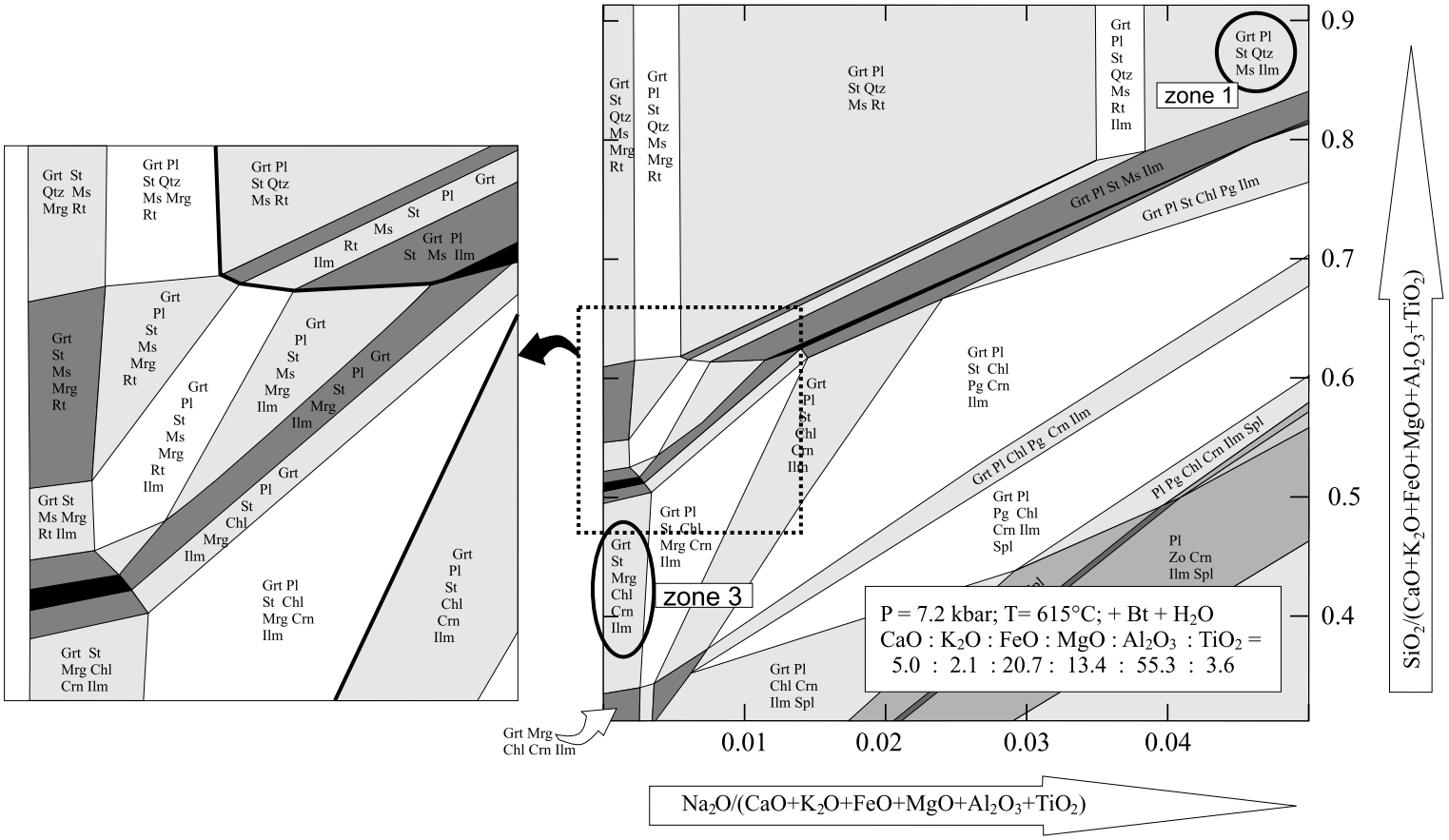

Fig. 6. X_{Na_2O}–X_{SiO_2} pseudosection in the model system NCKFMASH-TiO_2 at fixed pressure and temperature. Divariant fields are white, trivariant fields = light shading, quadrivariant fields = dark shading, pentovariant fields = black. The thick black line in the enlarged part (left hand diagram) is the margarite-out boundary. On the main diagram (at right) the stability fields of the parageneses of zones 1 and 3 are shown. They are shown by the black circled parageneses. Details of the choices for the axes are discussed in the text

axis. Corundum-bearing assemblages occur in all fields below about $X_{SiO_2} = 0.5$ for sodium free bulk compositions and below about $X_{SiO_2} = 0.75$ for $X_{Na_2O} = 0.05$. At extremely low SiO_2 contents, spinel and later zoisite and nepheline become stable, but they are outside the $X_{Na_2O} - X_{SiO_2}$ range of interest. The peak paragenesis of the country rocks in zone 1 occurs in a tri-variant field between $X_{Na_2O} = 0.04$ and 0.05 at silica contents above $X_{SiO_2} \sim 0.8$ in the upper right corner of the diagram. The fact that kyanite does not appear in this field is because the diagram was calculated for water saturated conditions. However, kyanite would be stable for this bulk composition by reducing the water activity to 0.8 (Fig. 5c). The corundum-bearing peak paragenesis of zone 3 is stable for sodium absent bulk compositions at silica contents between $X_{SiO_2} = 0.35$ and 0.5 in the bottom left corner of the diagram. Quartz *and* corundum absent assemblages appear on Fig. 6 in a narrow range between $X_{SiO_2} = 0.5$ and 0.6 in sodium free bulk compositions and between $X_{SiO_2} = 0.75$ and 0.84 for $X_{Na_2O} = 0.05$. In summary, Fig. 6 shows that the generation of corundum-bearing rocks in zone 3 from a Plankogel type mica-schist of zone 1 is possible by metasomatic depletion of SiO_2 and Na_2O at constant *PT* conditions around 615 °C and 7.2 kbar.

Discussion

Figure 6 has shown that the metasomatism around the Lölling ultramafic body can be explained by a fluid infiltration driven depletion of silica and sodium from the surrounding regional metapelites. The question remains where this fluid might have come from. When interpreting Fig. 5 we have shown that the corundum-bearing zone 3 is likely to have been water saturated during formation of the zone, while the surrounding metapelites in zone 1 were much drier with $a_{H_2O} = 0.8$. This interpretation of zone 1 is consistent with interpretations of *Tenczer* and *Stüwe* (2003), *Habler* and *Thöni* (2001) and others who have shown that regional metamorphism of the Kor- and Saualpe during the Eo-Alpine metamorphic cycle occurred at strongly water undersaturated conditions.

We suggest that this additional water in zone 3 may have been derived from prograde Eo-Alpine dehydration of the previously serpentinised ultramafic body. The Plankogel series has been interpreted as a suture zone at the end of the Variscan or Permian cycles (*Frisch* et al., 1989). As such, large quantities of water were carried downward to great depths during subduction causing complete serpentinisation of ultramafic rocks (see also e.g. *Manning*, 1997). We also know that the regional metapelites were water undersaturated prior to the Eo-Alpine cycle (*Habler* and *Thöni*, 2001). Regional metamorphism at Eo-Alpine times will have caused massive dehydration of the ultramafic rocks due to the ''sudden'' liberation of water when crossing the dehydration reactions that breaks down serpentine to form talc, olivine or tremolite (Fig. 5a). We suggest that it is this breakdown reaction in the system $MgO–SiO_2–H_2O$ that was the principle triggering mechanism for the metasomatic process. Water liberated from the ultramafic rocks during their prograde deyhydration infiltrated the surrounding metapelites dissolving silica and causing the breakdown of plagioclase and muscovite to form margarite and ultimately corundum.

Conclusions

From our investigations of the reaction zoning around the Lölling ultramafic body in the Saualpe region of the eastern Alps we can conclude the following:

1. The reaction zoning around the ultramafic body may be divided into 4 zones including: (i) the country rocks of the Plankogel series (zone 1) with typical parageneses of Grt–Pl–St–Qtz–Ms–Bt ± Ky; (ii) a transition zone (zone 2) with typical parageneses of Ky–St–Grt–Bt–Ms ± Pg ± Qtz ± Pl; (iii) a zone containing spectacular corundum-garnet rocks with the typical parageneses of Crn–St–Grt–Bt–Chl–Mrg and (iv) the ultramafic body itself (zone 4). However, outcrop is too sparse to recognize symmetry or asymmetry in the zonation.
2. The contact metasomatic process that formed this reaction zoning occurred during Eo-Alpine regional metamorphism at around 7.2 kbar and 615 °C. The water activity of the regional metapelites during this time was around 0.8.
3. Analysis of the bulk compositional variation across the reaction zoning shows that the metasomatic process is not caused by silica depletion alone, but that several elements must have moved simultaneously. The mass loss of zone 2 is of the order of 43% and in zone 3 up to 68%. Such significant mass loss and the width of the alteration zones over tens of meters suggests that the formation process was infiltration rather than diffusion metasomatism.
4. Calculation of thermodynamic pseudosections shows that the paragenesis of zone 3 may be explained with an X_{Na_2O}–X_{SiO_2} pseudosection. This section shows that corundum formation in contact metasomatic alteration haloes between ultramafic bodies and metapelites may be explained by a simultaneous depletion of Na_2O and SiO_2.
5. We suggest that the metasomatic process is driven by water liberated from the ultramafic serpentinites during prograde Eo-Alpine metamorphism of the Plankogel series. This is consistent with regional knowledge of the Plankogel series that all rocks are generally dry and also consistent with the fact that serpentinites contain much larger amounts of structurally bound water than the surrounding metapelites.

Acknowledgements

This project was supported by Acciones Integradas project 19/2001 of the Austrian Academic Exchange service OeAD as well as by project P-15474 of the Austrian Science foundation (FWF). *J. Connolly* and *R. Powell* are thanked for their positive and constructive reviews of an earlier version of this manuscript. *I. Scrimgeour* and *E. Schmädicke* are thanked for their reviews. *F. Koller* is thanked for his interest and cooperation during this study.

References

Baumgartner LP, Olsen SN (1995) A least-squares approach to mass transport calculations using the isocon method. Econ Geol 90: 1261–1270

Bebout GE, Barton MD (2002) Tectonic and metasomatic mixing in a subduction-zone melange: insights into the geochemical evolution of the slab-mantle interface. Chem Geol 187: 79–106

Carswell DA, Curtis CD, Kanaris-Sotiriou R (1974) Vein metasomatism in peridotite at Kalskaret near Tafjord, South Norway. J Petrol 15: 383–402

Cartwright I, Barnicoat AC (1986) The generation of quartz-normative melts and corundum-bearing restites by crustal anatexis; petrogenetic modelling based on an example from the Lewisian of North-west Scotland. J Metam Geol 4: 79–99

Emani M, Zang Q (1988) Magnesian staurolite in garnet-corundum rocks and eclogite from Donghai district, Jiangsu province, east China. Am Mineral 73: 48–56

Frisch W, Schmerold R, Neubauer F (1989) Die Plankogelserie eine ophiolithische Sutur. Arbeitstagung Geol BA, Wien, pp 34–41

Frey M, Desmons J, Neubauer F (1999) The new metamorphic map of the Alps; 1:500000; 1:1000000; Schweizer Mineral Petrogr Mitt, Bull Suisse Mineral Petrogr 79: p 230

Grant JA (1986) The isocon diagram – a simple solution to Gresens' equation for metasomatic alteration. Econ Geol 81: 1976–1982

Gregurek D, Abart R, Hoinkes G (1997) Contrasting eoalpine P-T evolutions in the southern Koralpe, Eastern Alps. Mineral Petrol 60: 61–80

Gresens RL (1967) Composition-volume relationships of metasomatism. Chem Geol 2: 47–55

Habler G, Thöni M (2001) Preservation of Permo-Triassic low-pressure assemblages in the Cretaceous high-pressure metamorphic Saualpe crystalline basement (Eastern Alps, Austria). J Metam Geol 19: 679–697

Hauy RJ (1822) Traite de Mineralogie 2nd ed, 594 pp

Hippertt JF (1998) Breakdown of feldspar, volume gain and lateral mass transfer during mylonitisation of granitoid in a low metamorphic shear zone. J Struct Geol 20: 175–193

Holland JTB, Powell R (1998) An internally consistent thermodynamic data set for phases of petrological interest. J Metam Geol 16: 309–343

Kretz R (1983) Symbols for rock-forming minerals. Am Mineral 68: 277–279

Lopez V, Soto JI (2002) Reaction zones developed between corundum metapelite and marble, Alboran Sea basement, western Mediterranean; origin and phase relations. Can Mineral 40: 85–101

Manning CE (1997) Coupled reaction and flow in subduction zones: Silica metasomatism in the mantle wedge. In: *Jamtveit B, Yardley BWD* (eds) Fluid flow and transport in rocks. Chapman and Hall, London, pp 139–169

Meixner H (1967) Neue Mineralfunde in den österreichischen Ostalpen XXII. Carinthia 77: 88–91

Miller C (1990) Petrology of the type locality eclogites from the Koralpe and Saualpe (Eastern Alps), Austria. Schweiz Mineral Petrogr Mitt 70: 287–300

Pfeifer HF (1987) A model for fluids in metamorphosed ultramafic rocks. IV. Metasomatic veins in metaharzburgites of Cime di Gagnone, Valle Verzasca, Switzerland. NATO ASI Series; Series C: Mathematical and Physical Sciences 218: 591–632

Powell R, Holland TJB (1988) An internally consistent thermodynamic dataset with uncertaintities and correlations. 3. Application methods, worked examples and a computer program. J Metam Geol 6: 173–204

Ranson P, William A (2000) Margarite-corundum phyllites from the Appalachian orogen of South Carolina; mineralogy and metamorphic history. Am Mineral 85: 1617–1624

Riesco M, Stüwe K, Reche J, Martinez F (2004) Silica depleted melting of pelites. Petrogenetic grid and application to the Susqueda Aureole, Spain. J Metam Geol (in press)

Robl J, Stüwe K, Fritz H, Bernhard F (2004) Cyclic fluid infiltration in structurally controlled Ag–Pb–Cu occurrences: (Schladming, Eastern Alps). Chem Geol 205: 17–36

Sandford RF (1982) Growth of ultramafic reaction zones in greenschist to amphibolite facies metamorphism. Am J Sci 282: 543–616

Shaw RK, Arima M (1998) A corundum-quartz assemblage from the Eastern Ghats granulite belt, India; evidence for high P-T metamorphism? J Metam Geol 16: 189–196

Schmerold R (1988) Die Plankogelserie im ostalpinen Kristallin von Kor- und Saualpe (Kärnten Steiermark – Österreich) als ophiolithische Sutur. Thesis, University of Tübingen, Germany, p 161

Schuster R, Frank W (2000) Metamorphic evolution of the Austroalpine units east of the Tauern Window: indications for Jurassic strike slip tectonics. Mitt Geol Bergbaustud Österr 42: 37–58

Simandl GJ, Paradis S (1999) Ultramafic-related corundum (contact metamorphic/ metasomatic). In: *Simandl GJ, Hora ZD, Lefebure DV* (eds) Selected British Columbia mineral deposit profiles, vol 3. Industrial minerals and gemstones Open File – British Columbia. Geological Survey Branch, pp 123–127

Stüwe K, Powell R (1995) PT-paths from modal portions. Application to the Koralm complex, Eastern Alps. Contrib Mineral Petrol 119: 83–93

Stüwe K (1998) Heat sources of Cretaceous metamorphism in the Eastern Alps; a discussion. Tectonophysics 287: 251–269

Surour AA, Arafa EH (1997) Ophicarbonates; calichified serpentinites from Gebel Mohagara, Wadi Ghadir area, Eastern Desert, Egypt. J Afr Earth Sci 24: 315–324

Tenczer V, Stüwe K (2003) The metamorphic field gradient in the eclogite type locality, Koralpe region, Eastern Alps. J Metam Geol 21: 377–393

Thöni M, Jagoutz E (1992) Some new aspects of dating eclogites in orogenic belts: Sm–Nd, Rb–Sr, and Pb–Pb isotopic results from the Austroalpine S-alpe and Koralpe type locality (Carinthia, Styria, southeastern Austria). Geochim Cosmochim Acta 56: 347–368

Thöni M, Miller C (1996) Garnet Sm–Nd data from the Saualpe and the Koralpe (Eastern Alps, Austria): chronological and P-T constraints on the thermal and tectonic history. J Metam Geol 14: 453–466

Weissenbach N (1975) Gesteinsinhalt und Seriengliederung des Hochkristallins in der Saualpe. Clausth Geol Abh Sonderb 1: 61–114

Wilson M (1989) Igneous petrogenesis. Unwin Hyman, London 466 pp

Authors' addresses: *K. Stüwe* (corresponding author; e-mail: kurt.stuewe@uni-graz.at), Institute of Earth Science, University of Graz, Heinrichstrasse 26, 8010 Graz, Austria; *M. Riesco* and *J. Reche*, Department of Geology, Universitat Autonoma de Barcelona, Edifici C Sur, 08290 Bellaterra, Spain